CHALMERS

Analysis, Design and Build of RC Composite Flying Wing

Project Course TME131

JOHN BORENIUS
TOBIAS BREDENBERG
NICHOLAS OTWAY
MARCUS RINGSTRÖM
BJÖRN WALLIN

CHALMERS UNIVERSITY OF TECHNOLOGY
Gothenburg, Sweden 2019

Abstract

A flying wing model is analyzed, improved and manufactured out of carbon fibre epoxy composite using resin infusion. With computational fluid dynamics (CFD) and finite element analysis (FEA), the angle of attack and composite layup of the wing is analyzed. The main goal of the project was to increase the lift to drag while maintaining the same weight or reducing weight while maintaining the lift-to-drag ratio. However, this objective changed to simply analyzing the aerodynamic differences between designs. The initial geometry was obtained from an online source [11]. The winglets were modified two times Firstly to remove sharp corners and incorporate a swept surface. The winglets were later removed altogether to enable milling of the plug, used for the resin infusion process. Turbulence was modelled by using the SST k-ω model which is a RANS model suitable for external aerodynamic flows with large separations to provide a good compromise between accuracy and computational cost. The study showed that when removing the winglets drag increased by 5.8% and the lift decreased by 7.8%. At the submission date of this report, no flight ready prototype exist however the main body of the plane is assembled and a test flight is planned to be carried out prior to the oral presentation of this project.

Contents

1 Introduction

This project involves the analysis and construction of a carbon fibre epoxy remote controlled (RC) flying wing. An existing wing design was chosen and downloaded from an online source [11], and modified to improve it's lift-to-drag ratio. The wing is simulated using commercial grade CFD- and FEA software packages. The manufacturing took place in the Chalmers composite lab. The project was divided into three parts.

1. CFD
2. FEA
3. Manufacturing

1.1 Purpose

The purpose of the project is to improve the lift-to-drag ratio of an existing RC flying wing geometry, illustrated in Figure 1.1.1. The RC wing will be constructed from carbon fibre epoxy and at least one design iteration is to be carried out where lift-to-drag is prioritized.

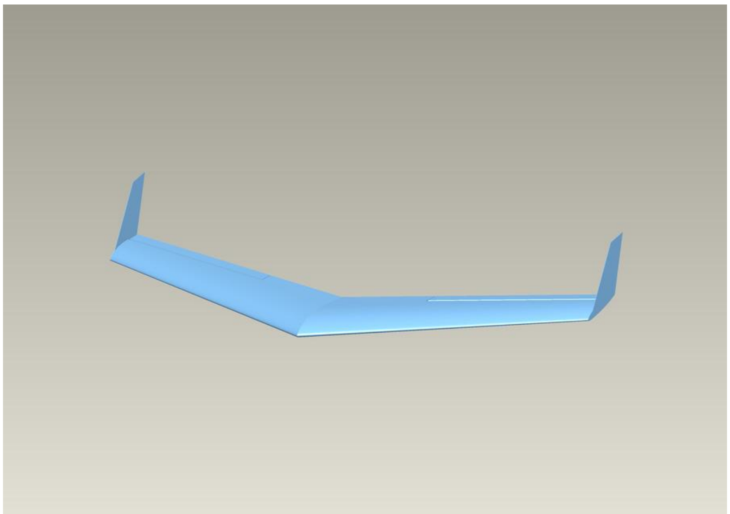

Figure 1.1.1: *The selected CAD model from grabCAD [18]*

.

1.2 Limitations

Due to the time restriction of 7 weeks a number of potentially important factors will be limited. Minor studies in static flight dynamics will be conducted to ensure longitudinal stability and prevent the wing from pitching up uncontrollably, however no extensive dynamic studies will be carried out. The CFD simulations will be limited to a RANS model, where the wing is in a cruising phase. Resin infusion will be used as the manufacturing method for the carbon fiber parts. The materials will be restricted to the unidirectional carbon fibre and epoxy matrix provided in the Chalmers composites lab as well as consumables provided for the resin infusion. The structural analysis of the wing will ensure that the weight of the airplane is low enough to sustain flight while not exceeding the maximum stress criterion of the carbon fiber laminate. Other failure modes such as fatigue, will not be included in the study. Motors, batteries and flight controllers are selected and provided by the university and will not be further analyzed or optimized.

2 Aerodynamic Theory

2.1 Stability Analysis

To assess the aerodynamic stability of the flying wing we first define three key locations that lie at certain positions along the chord line at the root of the wing.

1. The center of pressure, x_{cp}, is the point along the chord line at which the resultant force of the surface pressure field is acting through. This includes all flow induced lift and drag loads. The location of x_{cp} varies with angle of attack.

2. The center of gravity, x_{cg}, is the point on the chord line where the net downward force due to gravity is acting through. The sweep angle of the wing geometry means that the location x_{cg} does change slightly with different angles of attack. Since the variation is small in this case we can consider x_{cg} to be fixed in position.

3. The aerodynamic center, x_{ac}, is a single point that exists along the chord line, about which the pitching moment always remains constant and is independent of angle of attack.

Please note that this analysis is limited to static stability for pitch rotation about the z-axis only. Roll and yaw rotation are not considered.

2.1.1 Center of Gravity

A swept wing geometry forces the center of gravity to shift along the chord length towards the trailing edge. This has a great effect on the lever arm of any pitching moment that acts about x_{cg}. The conditions for stable flight can only be met if disturbances due to external loads are opposed by a tendency of the wing to return to its equilibrium position. This poses a fundamental design challenge in the case of flying wings, since we require $x_{cg} < x_{ac}$ to maintain positive static stability [2] The location of x_{cg} for a flying wing can be estimated with the following relation:

$$x_{cg} = \frac{l_r}{4} + \frac{2b}{3\pi} \tan \varphi_{0.25} \tag{2.1.1}$$

where l_r is the root chord length, b is the wing span and $\varphi_{0.25}$ is the sweep angle taken at the quarter-chord [12]. The approximate location of the center of gravity for this design case is found to be $x_{cg} = 0.20\text{m}$.

2.1.2 Longitudinal Static Stability

The wing is be considered to have positive static stability if it has a natural tendency to return to its equilibrium position following a disturbance by the forces and moments acting upon it [1]. The equilibrium position is where the wing is travelling with steady, horizontal, forward motion with zero net moment about x_{cg}. Since the wing altitude is constant we have $C_L = 0$ and since the pitching moment is zero we have $C_M = 0$. This mode of flight is called *trimmed* and the corresponding angle of attack is called the *trim angle*, α_e. The trim angle can be identified from the lift curve of the airfoil profile that corresponds to the wing design shown in Figure 2.1.1. Because the induced effects that cause 3d wings to behave differently from their 2d counterparts do not occur when $C_L = 0$ it follows that their curves share the same value for α_e [2].

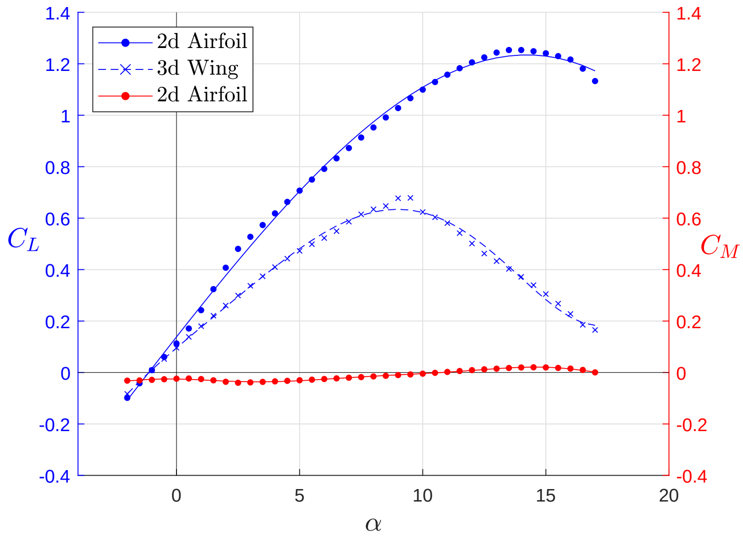

Figure 2.1.1: *Lift and moment curve for NACA 1412 airfoil and lift curve approximation for 3d swept wing.*

Consider a flying wing that is moving in a trimmed state. Suddenly, it is disturbed by a gust of wind which causes a change small change in α. A small increase in α is equivalent to a positive (nose up) pitching motion about x_{cg} while a small decrease in α is equivalent to a negative (nose down) pitching motion about x_{cg}. The shape of the C_M curve determines the static response of the wing. Let us assume that the C_M curve has a negative slope at α_e as seen in the left had side plot of Figure 2.1.2. Any small increase in α will produce a nehative moment about x_{cg} where $C_M < 0$, while any decrease in α will produce a moment that acts in the positive direction.

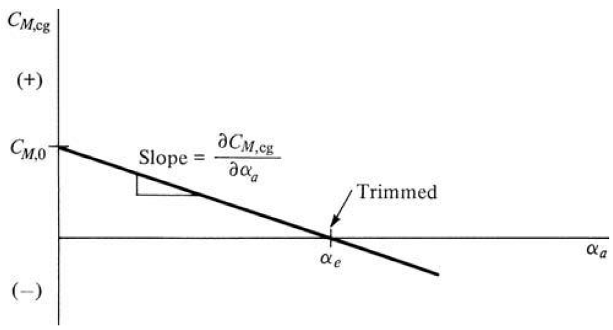

(a) *Negative slope.*

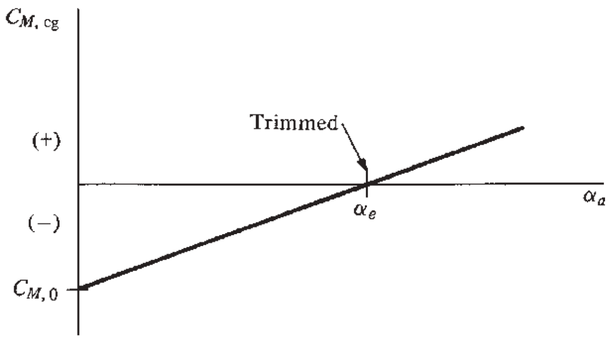

(b) *Positive slope.*

Figure 2.1.2: *Sample C_M curve with negative slope and positive slope, [1].*

2.2 CFD

2.2.1 Turbulence Modelling

Applying Reynolds decomposition on the instantaneous quantities in the Navier-Stokes equations, i.e velocity and pressure), and then averaging the equations over a time-scale, an expression for the mean quantities of the flow is obtained. The linear terms in the Navier-Stokes equations are the mean over a certain time-scale, but decomposition over the non-linear terms yields a new term called Reynolds stress term. The Reynolds stress term is a symmetric second order tensor with nine components (six components when using symmetry) defined as [9]:

$$R_{ij} = \rho \overline{v_i' v_j'} \tag{2.2.1}$$

Equation 2.2.1 is non-linear due to the product of fluctuating velocities. These six components have to be modelled in order to close the system of equations, also known as the closure-problem. A turbulence model is therefore needed to close the system [9].

2.2.2 SST k-ω Turbulence Model

The most common RANS turbulence models are the k-ε- and the k-ω models. In k-ε model the transport equations for turbulent kinetic energy k and dissipation ε are solved. The ω term in the k-ω model is the specific dissipation rate proportional to dissipation, ε, and turbulent kinetic energy, k, (i.e $\omega \sim \frac{\varepsilon}{k}$). The major differences between the two models is the way in which the boundary layer is modelled. In k-ε model the boundary layer is resolved by using wall functions whereas the k-ω model can be applied throughout the boundary layer, including the viscous sublayer without damping functions. This is perhaps the biggest advantage with the k-ω model [7]. Another weakness with k-ε model (other than it needs near wall modifications) is that it over-predict shear stresses in adverse pressure gradient flows compared to the k-ω model, which gives improved performance for boundary layers under adverse pressure gradients [9]. The disadvantage with k-ω model is that it is dependent on the free stream value of ω [9]. The SST k-ω model combines the best features of k-ε-and k-ω models by using a blending function, F. This approach blends a k-ε model in the shear flow region with a k-ω model near the wall. When $F = 0$, the SST model smoothly switches to the shear region while it switches to the near wall region when $F = 1$ [9].

2.2.3 Near Wall Treatment

Because of the large velocity gradients prevailing at the wall the mesh needs to be sufficiently fine near the wall in order to resolve these sharp gradients. In order to correctly predict lift and drag coefficients the boundary layer should be resolved all the way down to the viscous sublayer, at $y^+ < 1$. y^+ is a dimensionless wall distance from the wall to the first wall grid node, the y^+-value is defined as [9]:

$$y^+ = \frac{u_\star y}{\nu} \tag{2.2.2}$$

In k-ω models, the recommended wall treatment is the all y^+ wall treatment formulation. The all y^+ wall treatment enables wall functions in the inertial sublayer at $y^+ > 30$ and a low y^+ formulation in the viscous region of the boundary layer [7]. If a cell lies between the viscous and inertial sublayer, the all y^+ formulation uses a blending function g defined as [7]:

$$g = e^{\frac{-Re_y}{11}} \tag{2.2.3}$$

Where Re_y is the wall distance Reynolds number [7]:

$$Re_y = \frac{\sqrt{k}y}{\nu} \tag{2.2.4}$$

k is the kinetic energy, y is the wall distance and ν is the kinematic viscosity. In all y^+ formulation the reference velocity, $u_\star$, is defined as [7]:

$$u_\star = \sqrt{\frac{g\nu u}{y + (1-g)\sqrt{\beta^\star k}}} \tag{2.2.5}$$

where u is the velocity and $\beta^\star$ is a constant.

3 Method

3.1 Software

Three software packages used for this project: *SolidWorks* [16], *STAR-CCM+ 13.06.012* [6] and *ANSYS 19.1* [4]. Creation and editing of CAD models was done with *SolidWorks*. The FE analysis was carried out with the *ANSYS* add-on module *ANSYS Composite PrepPost (ACP)* and the aerodynamic analysis with *STAR-CCM+ 13.06.012*.

3.2 CAD Geometry

The initial CAD geometry was downloaded from the *grabCAD* website [18], and is illustrated in Figure 1.1.1. The endplate winglets of the initial geometry contained sharp corners which were difficult to mesh. Therefore, the model was modified in order to remove sharp corners and create smoother surfaces. The airfoil profile was changed to the NACA 1412 wing profile mentioned in Section 2.2. The resulting geometry is illustrated in Figure 3.2.1.

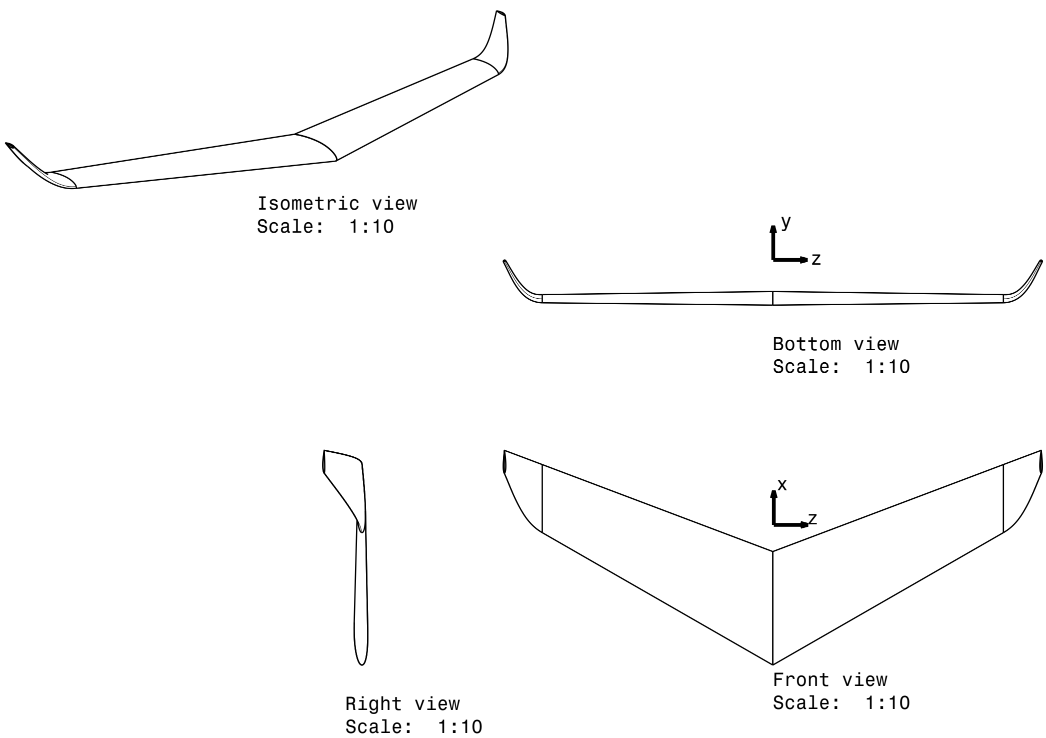

Figure 3.2.1: *Illustration of the improved geometry, which was simulated. The scale of the drawings is reduced to 1:20 to fit the report.*

During the manufacturing process the winglets of the geometry were modified a second time. The winglets were removed altogether in order for the model to fit in the mill. The final geometry without winglets is illustrated with measurements in Figure 3.2.2.

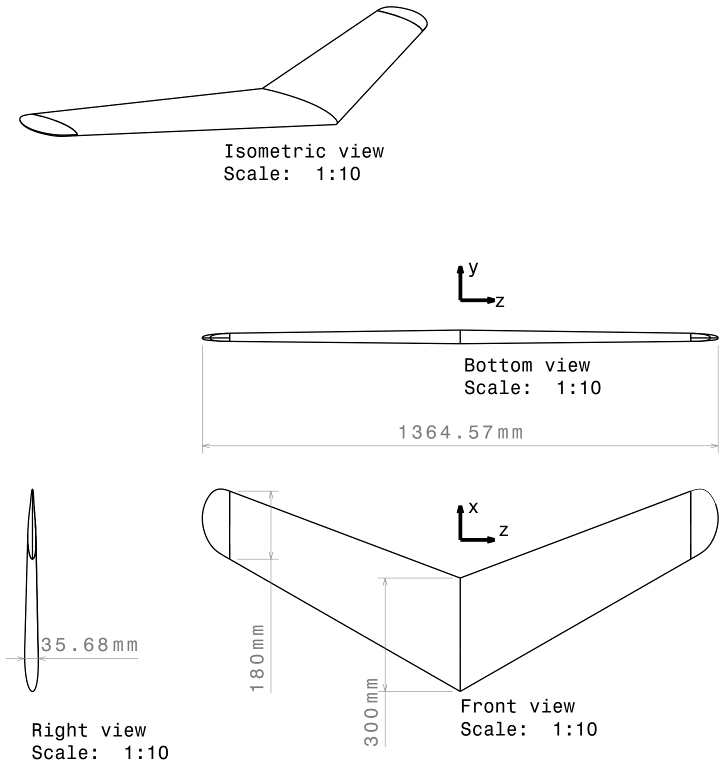

Figure 3.2.2: *Drawing of the second modification to the geometry which was simulated and used in the manufacturing. The scale of the drawings is reduced to 1:20 to fit the report.*

3.3 CFD modelling

Simulating stability of the flying wing can be complex and time consuming. In order to have time for the FEA and manufacturing the simulations only investigated one degree of freedom, the pitching angle. The flow in all simulations was therefore parallel with the top and bottom walls of the domain boundary. From the angle of attack study a lift curve was constructed in order to identify the critical angle where the wing starts to lose lift and the flow begin to separate. Turbulence is modelled using a modified RANS turbulence model, SST k-ω turbulence model. The SST model provides a good compromise between cost and accuracy and is suitable for adverse pressure gradient flows [9].

3.3.1 Case Setup

In order to obtain comparable results between the two design iterations. All cases (of varying angle of attack) are run with the same settings and cell count.

Geometry

Due to problems with poor CAD quality in the initial geometry, illustrated in Figure 1.1.1, meshing became a big issue leading to modifications of the geometry. Instead of endplate winglets with 90° angles the geometry is modified by integrating the winglets smoothly into the main body and increasing the rake angle of the winglets to facilitate meshing. The initial geometry is thus replaced by the geometry illustrated in Figure 3.2.1. Another design iteration is made where the geometry is modified to a geometry without winglets, illustrated in Figure 3.2.2. The comparative study is limited to see how lift and drag is affected with and without winglets. Trying to reduce the weight is not considered. The CAD model of the wing was constructed in *SolidWorks* based on a NACA1412 profile. The computational domain, (i.e the wind tunnel) is created as a 3D CAD model in *STAR-CCM+* and thereafter the wing CAD model is imported in *STAR-CCM+* as a surface mesh. The model is placed approximately five chord lengths (1.5m) in the x-direction and 2.5 chord lengths (0.75m) in the y-direction. To be able to specify boundary conditions on each part of the computational domain a fluid volume is constructed by subtracting the computational domain from the wing. In this way each part can be assigned to a region in the fluid volume. From the region a prescribed boundary condition can be applied to each part in the fluid domain.

Computational Domain & Boundary Conditions

To simulate the conditions of varying angle of attack, the geometry is rotated by implementing a coordinate system at the wing quarter-chord. The wing is then rotated to the new position obtaining the desired angle of attack. The wing is fixed at the wind tunnel left wall. The wind tunnel is divided into six different parts: inlet, outlet, left wall, right wall, bottom and top. At the inlet a velocity inlet boundary condition is used, which was calculated from XFOIL Reynolds number of 3×10^5, and a pressure outlet boundary condition of atmospheric pressure is used at the outlet. The wing surface is simulated as a stationary wall with a no slip boundary condition, ensuring that the velocity gradient is zero normal to the wall and that the relative motion between the fluid and the wall is zero. Bottom, top, left and right walls are set as symmetry planes. The computational domain and boundary conditions of the simulated wing are illustrated in Figure 3.3.1. Dimensions of the domain are listed in Table 3.3.1 and dimensions of the wing are illustrated in Figure 3.2.2.

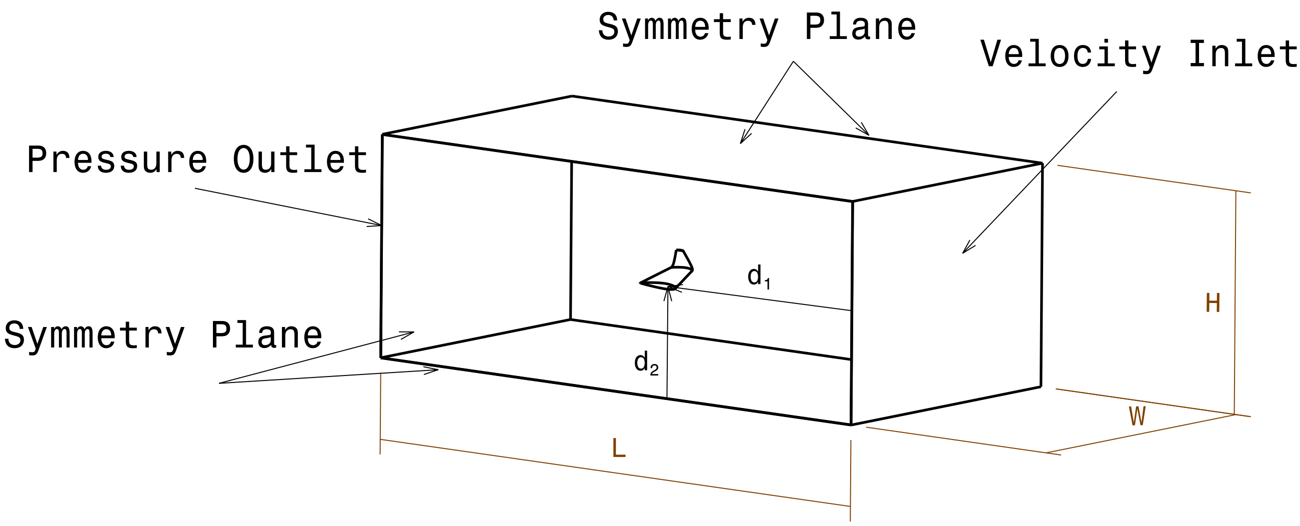

Figure 3.3.1: *Illustration of the computational domain and boundary conditions for CFD.*

The prescribed boundary conditions are summarized in Table 3.3.2.

Volume Mesh

From the imported surface mesh the *surface wrapper* is used to wrap the initial surface to provide a closed manifold, non-intersecting surface mesh [7]. In order to further improve the wrapped surface the *surface*

Dimensions	[m]
d_1	1.5
d_2	0.75
H	1.5
W	2
L	4
$chord$	0.3
$wingspan$	1.365

Table 3.3.1: Summary of computational domain dimensions.

Wing	Stationary wall	no slip
Wind tunnel inlet	Velocity inlet	
	Velocity magnitude	14.75 m/s
	Turbulence intensity	0.01
	Turbulent viscosity ratio	10
Wind tunnel outlet	Pressure outlet	0 Pa (101325 Pa reference)
	Turbulence intensity	0.01
	Turbulent viscosity ratio	10
	Backflow specification	Boundary - normal
Wind tunnel left wall	Symmetry plane	
Wind tunnel right wall	Symmetry plane	
Wind tunnel bottom	Symmetry plane	
Wind tunnel top	Symmetry plane	

Table 3.3.2: Summary of the prescribed boundary conditions. Note that the outlet pressure is from domain reference of atmospheric pressure, 101325 Pa.

remesher is used to provide the initial surface mesh into a high quality triangulated surface mesh suitable for CFD. The *trimmed cell mesher* produces a volume mesh by cutting a template mesh made out of hexahedral cells with the geometry surface [7]. The trimmed cell mesher is used when dealing with external aerodynamic flows due to its ability to refine the mesh in the wake region, which is a region of unsteady and turbulent fluid caused by boundary layer separation. In order to resolve the boundary down to the viscous sublayer and to handle the sharp velocity gradients prevailing close to the wall, the *prism mesher model* is used to generate prismatic cell layers adjacent to the wall boundaries, illustrated in Figures 3.3.2a and 3.3.2b. In CFD there is always a trade off between accuracy and computational cost. The wake region is thus limited to one chord length with 8° spread angle and the total volume mesh cell count is limited to approximately 5 million cells. In order to improve resolution in important areas most computational effort is placed in the wake region and in the near wall region where the largest flow gradients are expected [7].

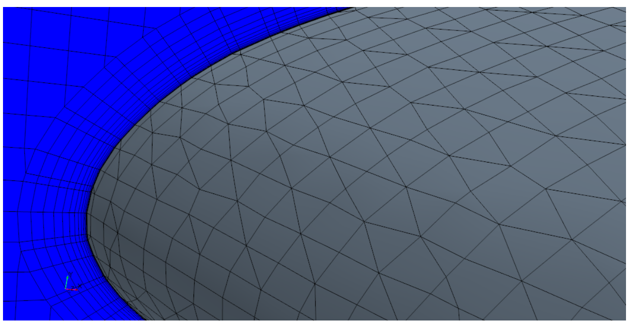

(a) *Prism layers at wing leading edge.*

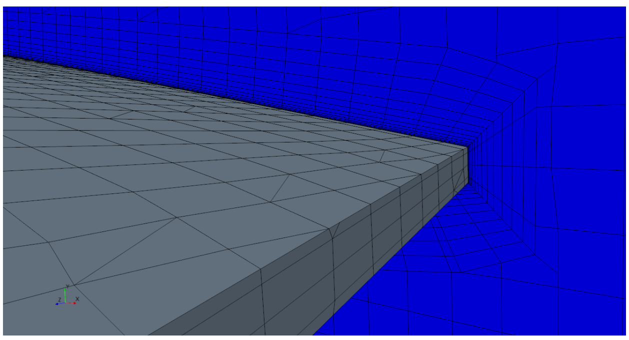

(b) *Prism layers at wing trailing edge.*

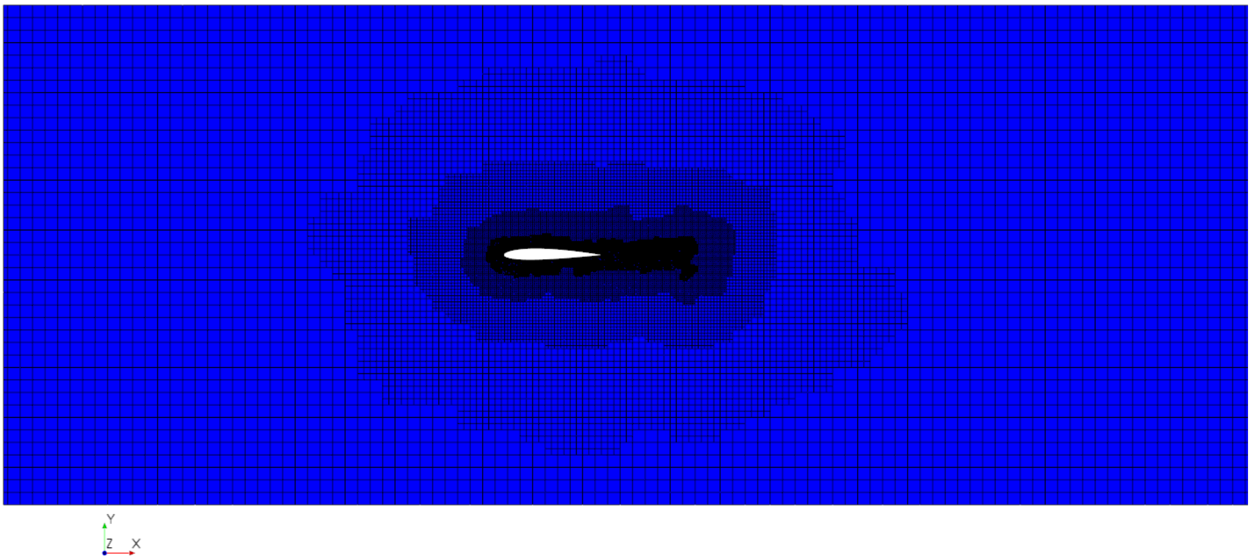

Figure 3.3.3: *Volume mesh illustrating the wind tunnel left wall and the wake region*

Physical Models

A brief overview of the most important models used in the simulation are outlined below

- **Spatial** - *Three dimensional*
- **Motion** - *Stationary*
- **Temporal** - *Steady state*
- **Flow** - *Segregated flow*: The segregated flow solver solves the equations of velocity (one for each velocity component) and pressure in an uncoupled manner. 2nd order upwind-scheme is used for the convection terms and the gradients are evaluated using Hybrid-Gauss LSQ with Venkatakrishnan gradient limiter.
- **Material** - *Gas* - Air
- **Equation of state** - *Constant density*
- **Viscous regime** - *Turbulent*
- **Turbulence model** - *RANS - SST Menter k-ω turbulence model*: A theoretical discussion about this turbulence model is provided in Section 2.3.1.
- **Near wall treatment** - *All y^+ wall treatment*: A theoretical discussion of the all y^+ wall treatment is provided in Section 2.3.3.

3.3.2 Convergence

The solution is monitored by checking convergence of residuals as well as plots of lift and drag coefficients. When lift and drag coefficients had variations less than 0.1% between 100 iterations, and the residuals dropped below 10^{-4} the solution was deemed converged. For large angle of attack however, lift and drag becomes increasingly more difficult to converge and the convergence criteria for lift and drag were therefore set to less than 1% of the minimum and maximum fluctuations, between an interval of 100 iterations.

3.4 FE Modelling

The wing was simulated without flaps while different composite layups were tested to analyze deflection and maximum stress. Other modes such as buckling or fatigue were not included due to time limitations. To further improve the model the mesh was refined in critical areas such as sharp bends and areas where a large pressure gradient was predicted. Since a heavy ($300g/m^2$) unidirectional carbon fibre matting (see Section 3.4.2) was provided, and weight was to be kept low, the layup possibilities were limited. With only one spanwise (0°, in the direction of the arrow in Figure 3.4.1) layer the structure had a maximum deflection in the order of $10^{-5}m$ which was deemed negligible. In order to maintain the airfoil shape of the wing it was decided to incorporate strips of carbon fiber in the travel direction of the wing (60°). Eight carbon strips covering 16% of the structure was decided upon. In order to save time these strips were not modeled. Instead a ply covering the entire structure but with a thickness 16% of the actual material thickness was used in the model. Placement of the reinforcement strips is represented in pink in Figure 3.4.1

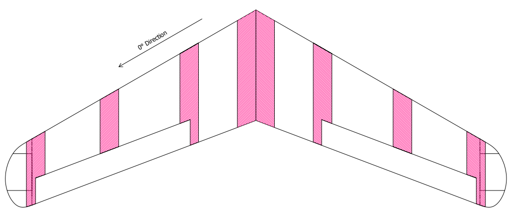

Figure 3.4.1: *Illustration showing the placement of the reinforcement strips.*

3.4.1 Loads & Boundary Conditions

The wing deflection was simulated with varying pressure applied in five zones spanning from the root to the wing tip. The pressure differential on the wing is continuous but due to ease of modeling and the prevailing time constraint, the pressure was divided into five zones. The pressure data was originally taken from *XFOIL* (see Section 2.2). In a later stage of the project the pressure data from *XFOIL* was replaced with pressure data from *STAR-CCM+*. The pressure data from the top and bottom halfs of the wings was summed and averaged in each zone and then applied to the top side of the wing. Boundary conditions can be seen in Figure 3.4.2 below.

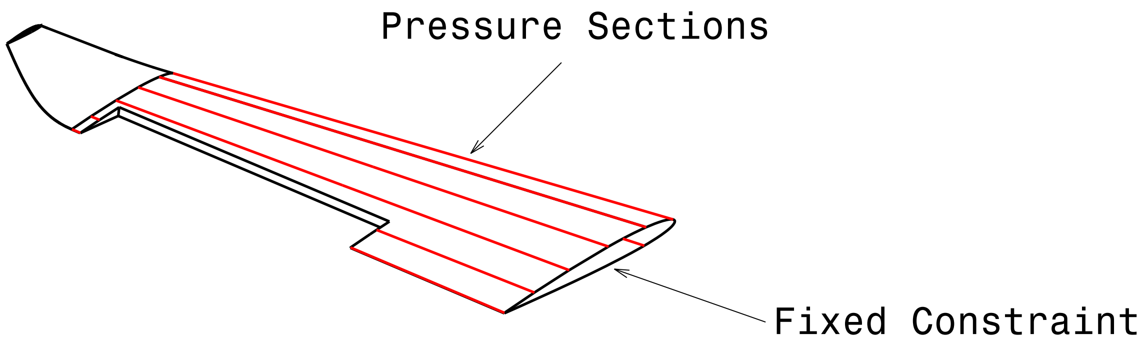

Figure 3.4.2: *Illustration of the loads and boundary conditions used in ANSYS.*

3.4.2 Material Data

The laminate used is *ZOLTEX PX35* stitched unidirectional carbon fibre, together with *NM Laminering 625* epoxy. Material properties for the carbon-fibre composite used in ANSYS are listed in table 3.4.1. The material properties for the epoxy and carbon fibre were provided by the project supervisor however they can also be obtained via the manufacturers, (see [8] and [17]). All unknown values were calculated with formulas from [10].

Table 3.4.1: Material properties for the carbon-fibre used in ANSYS and manufacturing.

Laminate properties	
Density	1.58 g/cm^3
Longitudinal Elastic Modulus (Tension)	110.25 GPa
Transverse Elastic Modulus (Tension)	14.7 GPa
Poisson's Ratio (LT)	0.31
Poisson's Ratio (TL)	0.0414
Shear Modulus (LT)	2.6 GPa
Shear Modulus (TT)	1.3 GPa
Axial tension strength	1.3 GPa
Axial compression strength	1.2 GPa
Transverse tension strength	0.043 GPa
Transverse compression strength	0.168 GPa
Shear strength	0.048 GPa

3.5 Manufacturing

The manufacturing process used resin infusion where dry fibres are placed in a mould which is then sealed with a vacuum bag. Resin is later drawn from a pot with the help of a vacuum pump at the opposite end of the mold. When all of the fibres are saturated the resin and vacuum lines are clamped off to stop the flow of resin while maintaining the vacuum and allowing the resin to cure. An example schematic of resin infusion can be seen in Figure 3.5.1.

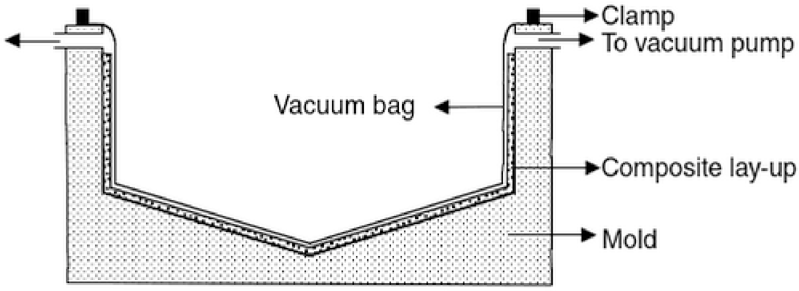

Figure 3.5.1: *Illustration of the infusion process, [5].*

Manufacturing started with the making of a plug on which the mould was to be created. Due to time limitations and delays no mould was created. For the airfoils resin was infused directly onto the plugs which makes the end product slightly larger than the original CAD model. The plug was divided into a top and bottom half in order to have the positive draft angle required for mould release. The plug was also divided at the symmetry plane due to size restrictions in the mill. In order to create the plug two sheets of $16mm$ thick, medium density fibre board (MDF) where glued together and milled with a computer numerical control (CNC) mill. The process is illustrated in Figure 3.5.2 and Figure 3.5.3. During milling a problem occurred because the mill was not stable enough to mill the winglets so the wing was quickly redesigned without winglets. The final design for manufacturing can be seen in Figure 3.2.2.

Figure 3.5.2: *Wing plugs being milled in the CNC-mill.*

Figure 3.5.3: *Plugs for one half of the wing.*

With the plug complete, coats of mould sealer and release agent were applied to prevent the parts from sticking to the plug, (see Figure 3.5.4). In Figure 3.5.5 carbon fibre mats were laid out on top of the plug in the directions explained in Section 3.4 and the resin infusion was carried out as seen in Figure 3.5.6. When the wings were taken off the plug it was discovered that buckling would likely become an issue. This was not foreseen since no regards to buckling was given during the modeling phase. In order to prevent buckling during flight a beam of extruded polystyrene was glued in the spanwise direction along the thickest part of the wing. With the beam in place a thin layer of *divinycell* foam was adhered to the inside of the symmetry edge to create a bonding surface for the glue. After the foam was installed the plane was glued and clamped together. In order to get a good bond between the top and bottom half along with a strong leading edge, a strip of bi-axial carbon fibre was laminated onto the leading edge.

Figure 3.5.4: *Plugs painted, sealed and prepared for carbon lay-up.*

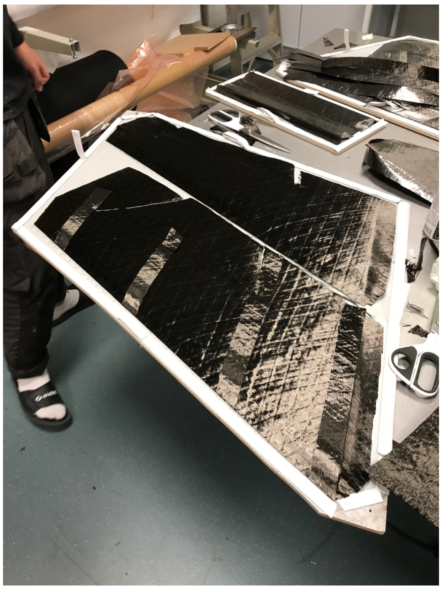

Figure 3.5.5: *Carbon lay-up, one* 0° *layer along the wing and some* 60° *strips perpendicular to the flight direction to reinforce and reduce shape distortion.*

Figure 3.5.6: *The beginning of the infusion process where the epoxy resin starts to flow through the part.*

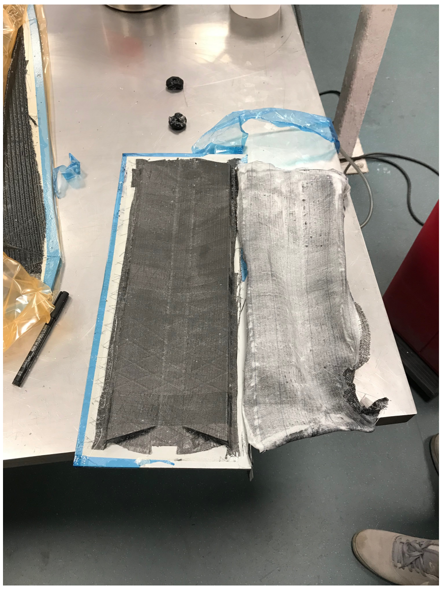

Figure 3.5.7: *Finished and cured wing flaps, the rough finish is due to the peel-ply and the positive mould.*

4 Results and discussion

4.1 CFD

4.1.1 Lift and Drag

The primary quantities required for assessing the flight characteristics of the wing are: lift coefficient, C_L, drag coefficient, C_D, moment coefficient, C_M and the location of the center of pressure, x_{cp}. Figure 4.1.1 illustrates the values C_L and C_D from the CFD simulations. It includes the results for the model with and without winglets. The results show that the design modifications of adding raked and canted winglets with a smooth transition from the main wing shape reduced the drag by 5.8% and increased lift by 7.8%, which shows that the design modification was a success. However, it is worth noting that the results are not validated by physical testing and are therefore not 100% reliable.

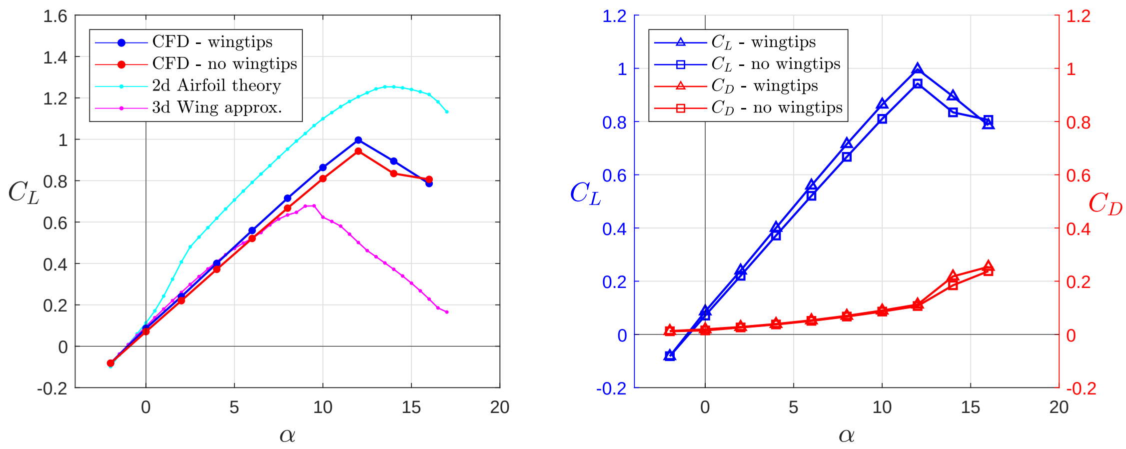

Figure 4.1.1: *CFD results for Lift and drag coefficients.*

Winglets are designed to modify the behaviour of the flow along the wing surface and in the wake region by suppressing wing tip vortices. When a wing generates lift a low pressure region develops at the upper surface and a high pressure region develops at the lower surface. The pressure gradient encourages flow at the edge of the wing to curl around its surface. This encourages separation and gives rise to rotational flow that develops into a trail of vortices left behind in the wake region as the wing continues its forward motion. This gives rise to a process known as *downwash* where several processes act to reduce the overall aerodynamic performance.

Firstly, the downward velocity component of the rotating flow disturbs the freestream flow, V_∞, causing an local reduction in the angle of attack. This transforms part of the vertical component of V_∞ into a horizontal component of V_∞, resulting in less lift and more drag. This is known as *lift induced drag* [2]. Additionally, the kinetic energy required to generate large vortices is supplied by the wing itself, since it is constantly performing work on the flow due to its forward motion. The effects of downwash should be mitigated by the presence of the winglet, however there is only a very small difference in the lift and drag results between the two models, as shown Table 4.1.1. A possible explanation may be that the freestream velocity, V_∞, is too low to bring about significant differences.

Wing Type	α^*	C_L	C_D	C_L/C_D	C_M	Reference area $[m^2]$
Tipped	12	0.996	0.112	8.872	-0.147	0.019117
Flat	12	0.943	0.107	8.830	-0.154	0.018854

Table 4.1.1: Aerodynamic quantities at the critical angle of attack, α^*.

The left hand side plot in Figure 4.1.1 provides a comparison of C_L between the CFD results and the predicted value based on lifting-line theory and 2d airfoil data. Although the critical angle is well underestimated the curves do show close agreement for angles of attack of roughly $\alpha < 8$. As illustrated in Figure 4.1.1 the lift-to-drag ratio decreases at 14 degrees angle of attack and this drop in lift to drag is investigated further. By comparing streamlines at 12 and 14 degrees angle of attack the flow structure can be analyzed. Streamlines for the tipped geometry is compared in Figure 4.1.2. The streamlines in Figure 4.1.2b are seen detaching from the airfoil and becoming turbulent. The same streamlines are also illustrated from the side in Figure 4.1.3. In Figure 4.1.3b the streamlines are seen recirculating and the flow separation is illustrated. The skin friction coefficient is also compared to confirm the flow separation at 14 degrees angle of attack, as illustrated in Figure 4.1.4.

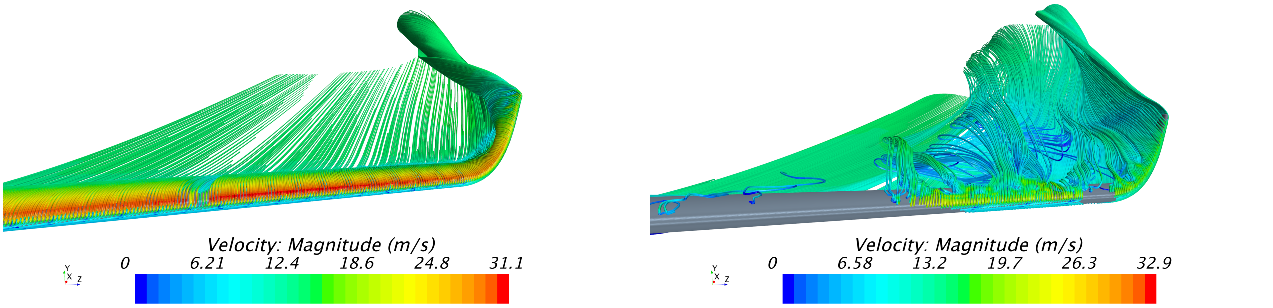

(a) *12 degrees angle of attack.*

(b) *14 degrees angle of attack.*

Figure 4.1.2: *Streamline comparison between 12 and 14 degrees angle of attack with winglets.*

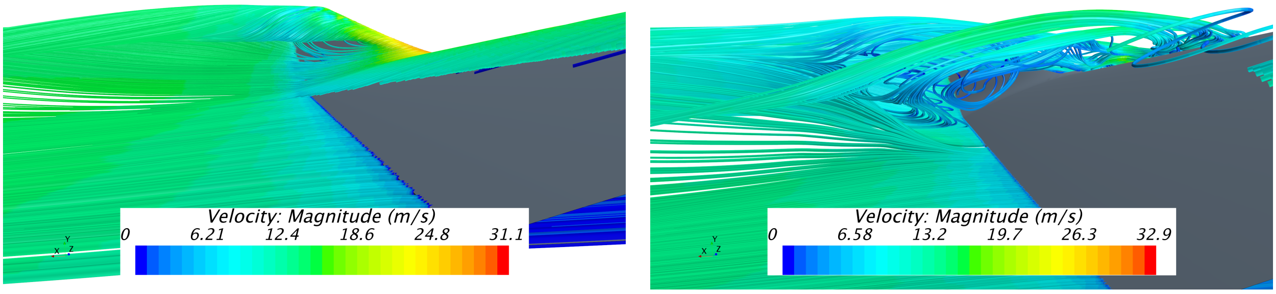

(a) *12 degrees angle of attack.*

(b) *14 degrees angle of attack.*

Figure 4.1.3: *Streamline comparison from the side between 12 and 14 degrees angle of attack with winglets.*

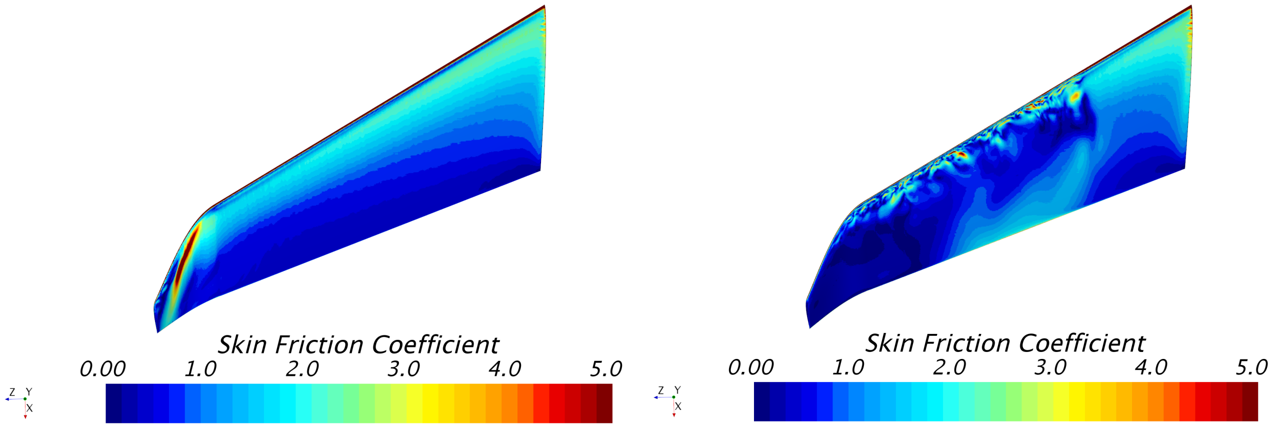

(a) *12 degrees angle of attack.* (b) *14 degrees angle of attack.*

Figure 4.1.4: *Skin friction coefficient comparison between 12 and 14 degrees angle of attack.*

In Figure 4.1.4b the skin friction coefficient is seen to be irregular and smooth in different regions of the wing surface. The irregular behaviour of the skin friction coefficient indicates the boundary layer has switched from laminar to turbulent. The modified geometry without winglets, which was manufactured, is also investigated. The skin friction coefficient is illustrated in Figure 4.1.5. The skin friction coefficient for the geometry without winglets is similar to the one with winglets (see Figure 4.1.4b). Streamlines are compared for the geometries with and without winglets to study the tip vortex. The streamlines are compared in Figure 4.1.6. In Figure 4.1.6b, tip vortex placement affects the lift generating surface, while including winglets is seen to supress the tip vortex from the lift generating surface, 4.1.6a.

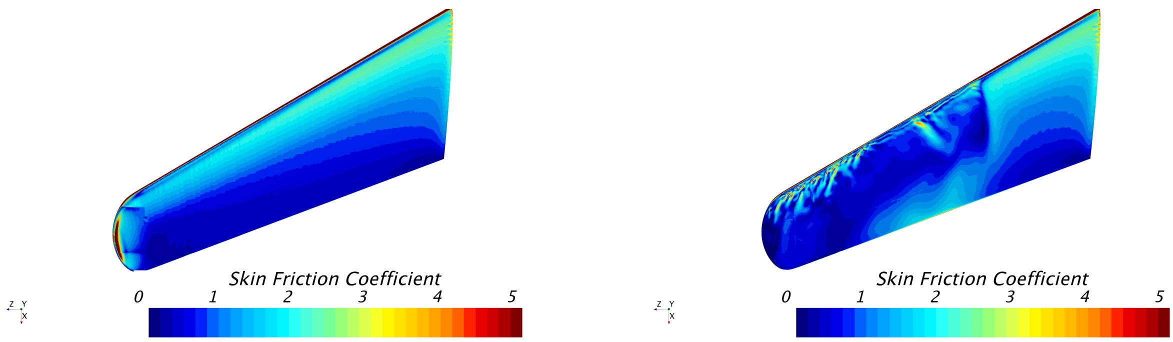

(a) *12 degrees angle of attack.* (b) *14 degrees angle of attack.*

Figure 4.1.5: *Skin friction coefficient comparison between 12 and 14 degrees angle of attack for the geometry without winglets.*

The skin friction coefficient for the geometry without winglets is similar to the one with winglets as shown in Figure 4.1.4b. Streamlines are compared for the geometries with and without winglets to study the tip vortex. The streamlines are compared in Figure 4.1.6. In Figure 4.1.6b tip vortex placement affects the lift generating surface and including winglets is seen to supress the tip vortex from the lift generating surface, shown in Figure 4.1.6a. The overall aerodynamic efficiency of an aircraft measured by the lift to drag ratio [1]. The CFD findings given in Table 4.1.1 shows that the difference between the two wing models is minuscule. The wing model featuring winglets is only 0.47% more aerodynamically more efficient than the model without winglets.

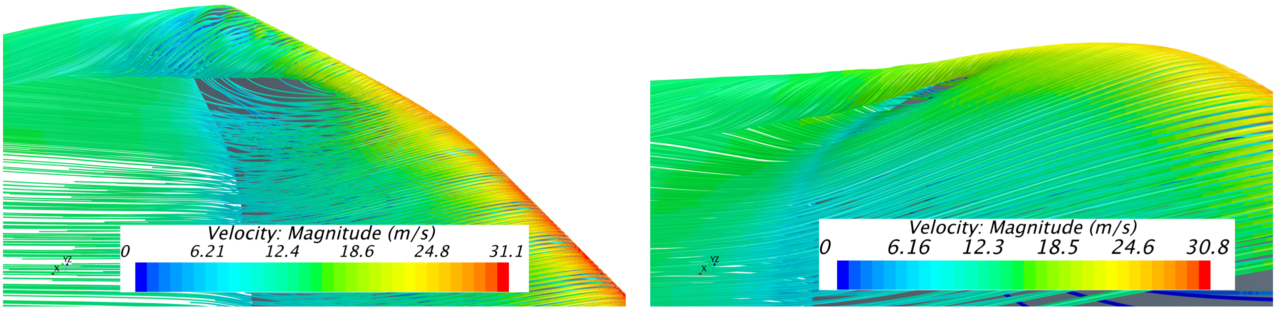

(a) *12 degrees angle of attack and with winglets.* (b) *12 degrees angle of attack and without winglets.*

Figure 4.1.6: *Streamlines illustrating the tip vortex are compared with and without winglets.*

4.1.2 Convergence

The reason for the oscillating behaviour mentioned in Section 3.3.2 could be due to that the flow situation become increasingly more transient for high angle of attacks. A stalled airfoil is characterized by boundary layer detachment and vortex formation in the wake region with a certain characteristic frequency. Due to the unsteady nature of these flow phenomena running a steady simulation on an unsteady problem may be a reason for the convergence issues. In order to enhance convergence a remedy could be to choose a scale-resolving turbulence model that is better at predicting boundary layer detachment and vortex formation, such as LES or DES SST k-ω model.

4.1.3 Moment Coefficient and Center of Pressure

The results for pitching moment coefficient, C_M, taken about x_{cg} are illustrated in the left hand side of Figure 4.1.7. The conditions for positive static stability that were stated at the end of Section 2.12 are not entirely satisfied. Although the C_M curve does have a negative gradient for all measured values of α up to the critical angle of attack, the moment at the angle of trim, α_e, is non-zero. This is an indication that the estimated center of gravity, x_{cp}, that was calculated using Equation 2.1.1 is not entirely accurate, since all moments are taken about the center of gravity by convention. The true center of gravity must lie a short distance closer towards the leading edge compared with the estimated location of $x_{cp} = 0.2m$, this is because C_M at α_e is a small negative value. If the true center of gravity is used to compute the moment coefficients the C_M curve in Figure 4.1.1 will shift upwards such that $C_M = 0$ at α_e. The flying wing can then be said to satisfy the criteria for positive static stability.

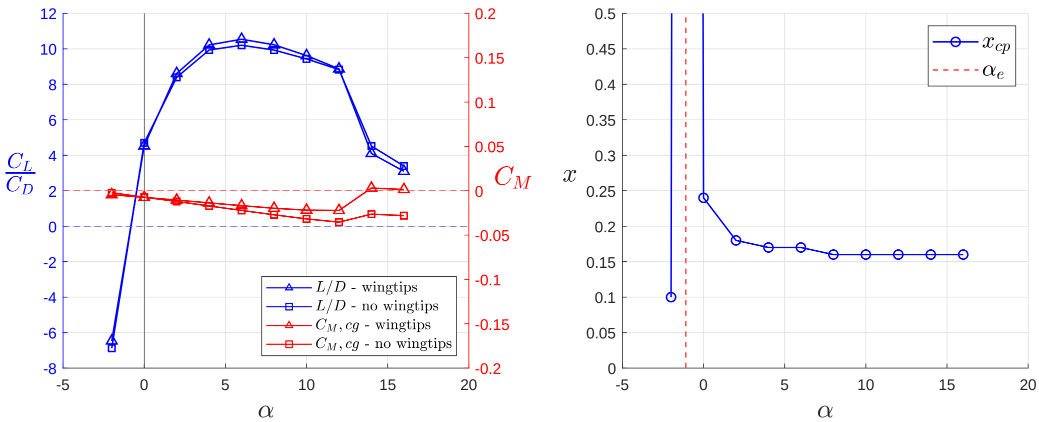

Figure 4.1.7: *CFD results for lift to drag ratio and moment coefficient (left), and center of pressure (right).*

The left hand side plot in Figure 4.1.7 shows hows the location of the center of pressure, x_{cp}, varies with angle of attack. It shows that that as the the wing approaches the point of zero lift at α_e, the center of pressure goes to infinity. This is expect to occur since the net pressure loads acting over the surface have no net vertical component which ultimately forces x_{cp} to lie *outside* the geometry of the wing [1]. The position of the center of gravity, x_{cg} , must also be considered with respect to the shift in x_{cp}. As the the wing pitches upwards x_{cp}, rapidly converges towards a location approximately 0.16m along the cord length. This is where the aerodynamic center, x_{ac}, is located since the pitching moment taken about this point remains constant and is independent of the angle of attack. As stated in Section 2.1.1, to maintain static stability we must ensure that the center of gravity is always located forward of the aerodynamic center. Therefore we require that $x_{cg} < 0.16$. This is consisted with the findings discussed in the previous paragraph which showed that the initial guessed value of $x_{cg} = 0.20$ must be reduced.

4.1.4 CFD Data Validation

The pressure coefficients from the CFD results for the tipped wing model were validated against their corresponding values obtained using XFOIL. This is illustrated in Figure 4.1.8 with each subplot featuring a different angle of attack. The vertical axis indicates C_P and the horizontal axis indicates the longitudinal position. The results generally show good agreement in high pressure regions (mostly along the lower surface) where $C_P > 0$ but poor agreement in low pressure regions where $C_P < 0$ (mostly along the upper surface). This is expected because the three-dimensional effects of flow separation that occur along the upper surface are not adequately captured by the idealised two-dimensional flow model that XFOIL uses. However, since the flow across the lower surface is mostly smooth and laminar the pressure field data for both cases provides a sufficient means of validation for the CFD simulation.

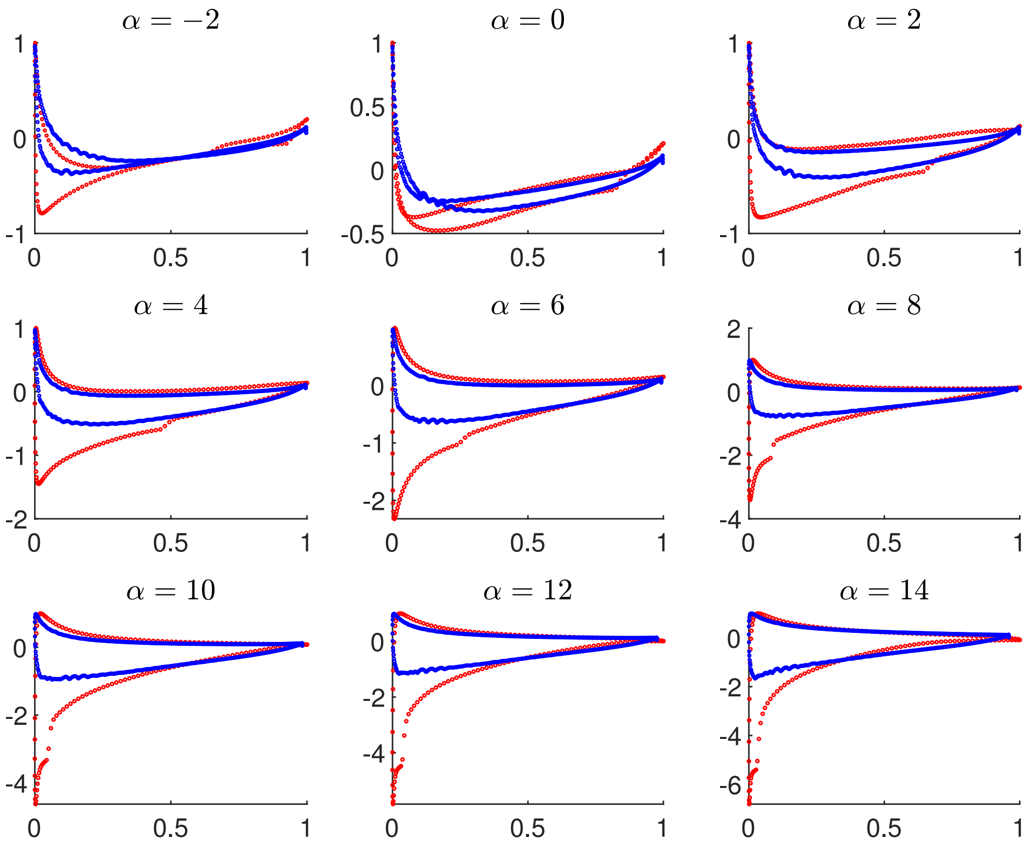

Figure 4.1.8: *Pressure coefficients for CFD (blue) and XFOIL (red).*

4.2 Structural

As mentioned in Section 3.4 the carbon fibre provided by Chalmers was very heavy, did not give many options for the lay up and deflection was negligible- even with a single ply of UD carbon. Due to the thick matting the wing was very stiff in bending as expected. However, a result that was neither foreseen while modeling or expected was the fact that the wing was buckling during handling. As predicted the stresses in the wing were well below the critical stress levels seen in Table 3.4.1 of the composite at a maximum of $11MPa$. Worth mentioning is that these stresses were achieved with a fixed boundary condition at the symmetry plane, which is not the case in real world flight since the plane will accelerate in the case of unbalanced forces. However, during flight the wing will be exposed to dynamic loading and shock loading which will be larger than the static loads presented for this case. Therefore the fixed boundary condition was deemed a good medium to predict stresses in the wing.

While analyzing future models buckling of the wing, faces should definitely be taken into consideration since this could present itself as an issue in the physical model. For future design and manufacturing work lighter UD matting and/or weave would be recommended so that the construction could be optimized and extra strength could be added to areas where the relative forces are large, such as the leading edge and attachment points for the flaps and motors

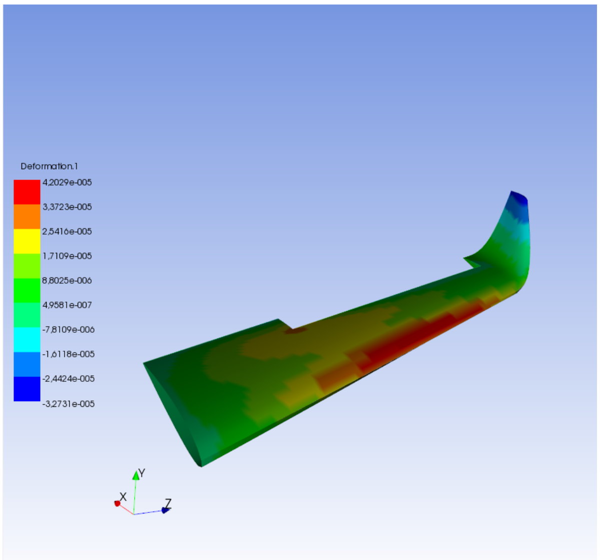

Figure 4.2.1: *Deflection due to pressure loads from the CFD simulation.*

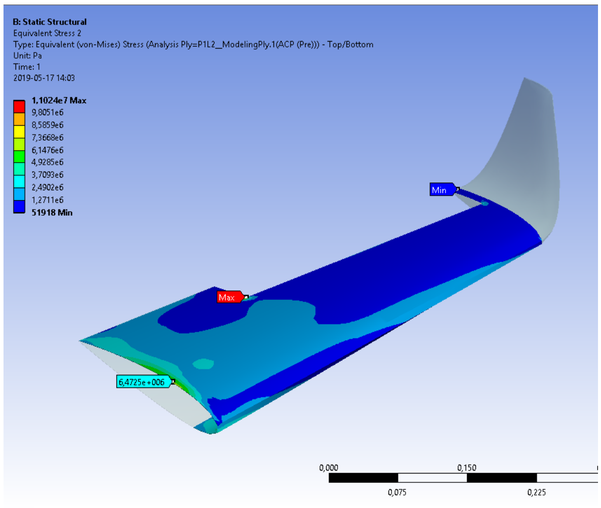

Figure 4.2.2: *The von Mises stress distribution over the wing.*

4.3 Manufacturing

The manufacturing process went according to plan (except from the redesign mentioned in Section 3.5) with a fully saturated laminate and little excess epoxy. Since a single layer of unidirectional carbon fibre was used for the majority of the plane, the wing surfaces were quite brittle while subjected to transverse tension and shear forces. This could be prevented in future work by using lighter weight fabrics in order to use multiple directions in the lay up. The final weight of the wing without hardware ended in 450 grams which is comparable to the estimations made in ACP toolbox which ended up at around 430 grams. In order to achieve a smoother outer surface and tighter tolerances the use of negative glass fibre moulds are recommended instead of using positive plugs for manufacturing. Dividing the plane into a top and bottom half instead of four parts as used for this project would also make for an easier assembly, a stiffer and lighter structure due to elimination of foam at the gluing surfaces, as well as a smoother manufacturing process in general. The carbon fibre structure of the wing was completed within the time frame. However, the wing in a final flying condition with all hardware mounted was not finished before the due date of this report. The aim is to arrange a test flight before the date of the final oral presentation.

Figure 4.3.1: *Two parts being glued together to form the complete bottom part.*

Figure 4.3.2: *Top and bottom part glued together to form the complete wing.*

5 Conclusion and further work

Data comparison between the CFD and XFOIL results, show that the CFD simulation provides a sufficiently accurate representation of reality under the prescribed flow conditions. The aerodynamic performance of the two flying wing models in terms of the lift to drag ratio is shown to be nearly identical. The wing design that includes winglets generates greater lift and less drag. Based on the stability assessment the wing should be capable of achieving a steady horizontal mode of flight as long as the center of gravity, x_{cg}, is located less than 0.16m along the root chord length. It is recommended that the manufacturing team use the additional weight added by the electronic components to shift x_{cg} forward to ensure that the stability requirements are satisfied.

For a comprehensive analysis of the aerodynamic behaviour of the flying wing it is suggested that additional flight velocities be investigated along with a dynamic stability analysis to assess the time dependent motion of the wing for all six degrees of freedom. Assessing the effect of varying the pitch of the wing flaps will also significantly effect the lift and drag characteristics. Additionally, the numerical analysis could be deepened to include a transient simulation, a grid independence study and an evaluation of different turbulence models.

For the manufacturing process it would have been better to make the left and right part in one piece for both rigidity and ease of assembly due to the minimization of glue joints. From the FE analysis it was clear that one layer of the supplied carbon mat would be enough to withstand the applied flight loads but the wing showed some buckling tendencies during handling and assembly. Cases like releasing it from the plug and over all handling and gluing was not considered and became an issue with some small longitudinal cracks in the carbon pieces due to the brittle nature of unidirectional fibres. Preferably the UD carbon mat should be lighter to enable the use of additional fibre directions while maintaining weight.

References

[1] J. D. Anderson Jr. *Introduction to Flight (ed.)* 2008.
[2] J. D. Anderson Jr. *Fundamentals of aerodynamics*. Tata McGraw-Hill Education, 2010.
[3] J. D. Anderson. *Aircraft performance and design*. McGraw-Hill Science/Engineering/Math, 1999.
[4] ANSYS. *ANSYS*. 2019. URL: `https://www.ansys.com` (visited on 05/20/2019).
[5] B. A. L. Broutman and K. Chandrashekhara. *Analysis and Performance of Fiber Composites*. 3rd. John Wiley & sons, New York, 2006.
[6] S. CCM+. *Star CCM+*. 2019. URL: `https://mdx.plm.automation.siemens.com/star-ccm-plus` (visited on 05/20/2019).
[7] *CD-Adapco. STAR-CCM+ Manual, version 13.06.012 edition.*
[8] *Datablad NM Laminering 625*. Nils Malmgren AB, 2011. URL: `http://www.nilsmalmgren.se/Datablad/TDS%5C%20S%5C%20NM%5C%20Laminering%5C%20625.pdf`.
[9] L. Davidson. *ebook: Fluid mechanics, turbulent flow and turbulence modelling*. Division of Fluid Dynamics, Chalmers University of Technology, 2019.
[10] M. Fagerström. *Lecture notes: Composite mechanics*. Division of Material and Computational Mechanics, Chalmers University of Technology, 2019.
[11] *GrabCad website*. Stratasys, 2019. URL: `https://grabcad.com/`.
[12] M. Hepperle. *Basic Design of Flying Wing Models*. May 2018. URL: `https://www.mh-aerotools.de/airfoils/flywing1.htm`.
[13] D. Kuchemann. "The aerodynamic design of aircraft". In: *Progress in aeronautical sciences, 1965, 6,271 (Pergamon, London)* (1978).
[14] L. K. Loftin. *Quest for performance: The evolution of modern aircraft*. 468. Scientific, Technical Information Branch, National Aeronautics, and Space ..., 1985.
[15] H. Y. Mark Drela. *XFOIL*. 2013. URL: `http://web.mit.edu/drela/Public/web/xfoil/` (visited on 05/20/2019).
[16] SolidWorks. *SolidWorks*. 2019. URL: `https://www.solidworks.com` (visited on 05/20/2019).
[17] *Technical datasheet. ZOLTEX PX35*. Zoltek, 2019. URL: `https://zoltek.com/products/px35/`.
[18] *Zagikiller flying wing*. Van Haren, B., 2013. URL: `https://grabcad.com/library/zagikiller-flying-wing-1?fbclid=IwAR3SF0qRZkOKqpY3LxbgFm-dgkItbUYyo0Q7n86ttpSIdnirNJk944XIgfQ`.

Contribution Report

The contribution of project members is summarized in lists.

Björn Wallin

- Contact person (Handling hand-ins and meeting notes).
- Planning report (Writing and revision of report with feedback).
- Support CFD part (Post-processing of CFD results).
- Test flight plan (Search for laws/requirements, suitable flight area and flight procedures).
- Final report (all parts except theory).

Marcus Ringström

- Together with Nicholas Otway responsible for pre-and post-processing, including meshing and case set up (choice of turbulence model, numerics etc).
- Responsible for setting up the cluster account including upload and monitor jobs on the cluster.
- Final report writing, mainly the CFD part, but also giving some assistance on the aerodynamic part.
- Involvement in the planning report together with the other members in the group.

Nicholas Otway

- Aerodynamic theory and stability analysis.
- Preliminary design estimations using simplified models and analytic calculations.
- Together with Marcus Ringström responsible for pre and post processing, including meshing and case set up.
- Data analysis and figure plotting.
- Report writing and editing.

John Borenius

- Model design and improvement.
- FE modelling.
- Manufacturing (Planning, milling, CAD/CAM, carbon fibre layup, resin infusion, glue up, final assembly).
- Electronics and programming.
- Planning report.
- Final report.

Tobias Bredenberg

- Model design and improvement.
- FE modelling.
- Manufacturing (Planning, milling, CAD/CAM, carbon fibre layup, resin infusion, glue up, final assembly).
- Electronics and programming.
- Planning report.
- Final report.

Learning Process

As mentioned during the feedback for the planning report, the project was ambitious to include both FEM and CFD simulations together with manufacturing. The time required for the meshing procedure was under predicted, mainly due to geometry imperfections, a more well defined geometry would facilitate the meshing process. The fact that we were somewhat inexperienced with *STAR-CCM+*, the learning curve was rather steep.

When working with products to be manufactured, the manufacturing process always needs to be in mind. The composite manufacturing was planned and deemed feasible. However, the creation of the mold was overseen, and the geometry had to be modified in order for the mill to handle the curvatures.

From the FEM results and intuition, the composite layup of one layer was believed to be sufficient. However, from the manufacturing it was realized that the wing became very brittle and extra layers would improve this.